ISSN 2176-5480

22nd International Congress of Mechanical Engineering (COBEM 2013)
November 3-7, 2013, Ribeirão Preto, SP, Brazil

EXPERIMENTAL STUDY OF HEAT TRANSFER ON RAPID PROTOTYPING BY ARC WELDING APPLIED TO AEROSPACE COMPONENTS

Felipe Ferreira Fraga
Guilherme Caribé de Carvalho
Universidade de Brasília - UnB, Faculdade de Tecnologia/Departamento de Engenharia Mecânica, Brasília DF, Brasil.
felipef22@gmail.com, gccarval@unb.br

Artyom Yurevich Andrianov
Dnipropetrovsk National University named after Oles Hochar – DNU, Physics and Technology Faculty/Department of technology, Dnipropetrovsk, Ukraine.
arean@inbox.ru

Abstract. *In this work the possibility to use rapid prototyping by arc welding for manufacturing of two pieces of a valve block of the rocket engine gas-hydraulic drive is studied. It was found that prototyping provides high material utilization or low amount of material turned to scrap comparing with traditional methods of manufacturing. Here also metallographic study is performed on a sample prepared by the prototyping emulating process. The materials used in process are martensitic stainless steel EP56 and austenitic stainless steel 08Kh21N10G6, created in the former Soviet Union and still widely used nowadays. Segregation of micro- and macrostructure was found in the sample, which occurred due to multiple thermal cycles of heat transfer.*

Keywords: *Rapid Prototyping; Arc Welding; Aerospace; Metallography; Thermal Cycle; Stainless Steels.*

1. INTRODUCTION

Rapid prototyping was born from the growing demand of industry to improve the design process by providing a means of producing partially functional prototypes for geometrical compatibility studies without the need to develop the manufacturing process for that part before knowing its final shape. Consequently, a new technological concept was developed in order to reduce the development time of prototypes in the initial stage of projects.

Unlike conventional processes such as machining, that involves the subtraction of material from the raw workpiece to obtain the desired shape, in rapid prototyping, the part geometry is attained by depositing successive layers of material. This is also known as “additive technology”.

The amount of different rapid prototyping systems found nowadays exceeds two tens (Volpato, 2007), but usually these processes are related to production of prototypes made of materials (polymers or special metal alloys) normally with different mechanical properties then those required in the final product, generally made of steel alloys and other metals alloys such as the ones based on aluminum, titanium, nickel, magnesium, etc, depending on the part application. Thus, they are useful just to visual and ergonomic evaluation, or manufacturing feasibility studies.

That way, a new model for rapid prototyping came to preclude such shortcoming. This is the rapid prototyping by arc welding, which could allow more realistic mechanical properties since the prototype is made from weldable materials similar or exactly equal to that of the final product.

In the process of rapid prototyping by arc welding, generation of prototypes is made directly from a 3D solid model created by a CAD system (Computer Aided Design). The technique consists from stages, such as creation of CAD model, dividing that model into successive layers and generation of a continuous trajectory, which must be followed by a torch guided by a robot. After the continuous deposition of material, the robot reproduces the virtual model into a real piece in a similar manner as the already established Fused Deposition Modeling (FDM) process, which uses a thermoplastic polymer as the building material.

The main difficulty of this kind of prototyping concerns the excessive heat accumulation due to various thermal cycles involved, which influence the geometry of the solid and the surface finish of the piece (Zhang *et al.*, 2002), being primordial the right choice of welding parameters and a path optimized for prototyping. The multiple thermal cycles are also the reason for the heterogeneity (segregation phases) found along the layers. Such structural heterogeneities provide different mechanical properties along the length of the material that must be carefully analyzed in order to determine, for example, the strength of the processed material.

Rapid prototyping by arc welding also found application in the aerospace area. Some studies confirm the possibility of using this technology to jet engine blade repair and to manufacturing small components (Thukaram, 2010). Titanium alloys, widely used in aerospace, has been used in rapid prototyping by arc welding to study their mechanical properties and the possible use of these components in aerospace (Brandl *et al.*, 2010; Baufled and Biest, 2006; Baufled *et al.*, 2011). In general, the mechanical tests show results similar to or even better than those produced by casting.

ISSN 2176-5480

Although some studies have been conducted on post-solidification phase transformations (Fachinotti *et al*., 2010; Skiba, Baufled and Biest, 2009), it is little known about the micro and macro-segregation that occurs along materials subjected to this prototyping. Such segregation may lead to significant local differences in the physical properties of solid materials with limited diffusion. While the micro-segregation has great influence on solidification cracking susceptibility the macro-segregation has influence on the amount of some phases in each layer (e.g. ferrite in stainless steels, which affects the crack resistance by solidification and corrosion) (Kou, 2003). That way, there is also a necessity to study in more detail the aspects and influences caused by segregation.

2. AEROSPACE APPLICATION

As the focus of this work is also a possible future use of this technology in the aerospace, comparative studies of the advantages of the use of rapid prototyping by arc welding in relation to traditional methods should be carried out.

That way, two methods of manufacturing by arc welding of two parts of the valve block component of the rocket engine gas-hydraulic drive unit (Fig. 1) were studied and compared with traditional manufacturing processes involving material removal (such as machining) in order to determine the highest possible material utilization. This is because such materials are usually expensive since they have a specific application with a high degree of reliability in which higher material utilization means less technology cost. The material used for this purpose is the 9Kh16N4B martensitic stainless steel, which was developed by the former Soviet Union and is still widely used in aerospace applications.

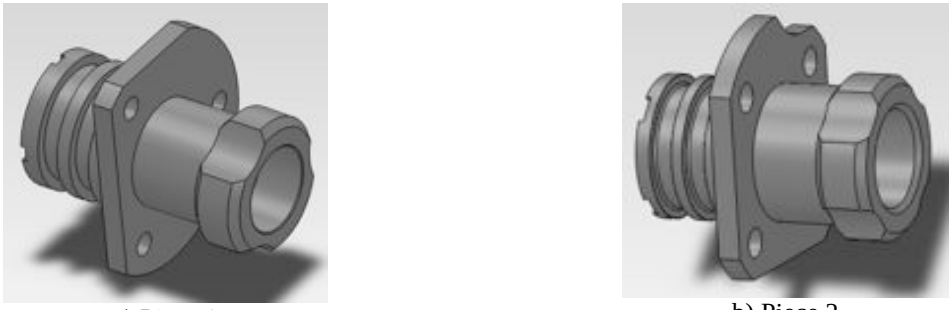

a) Piece 1 b) Piece 2

Figure 1. The body and the flange of valve block of the rocket engine gas-hydraulic drive unit.

For the traditional method of manufacturing, the parts to be manufactured should start from a cylindrical solid bar of 53 mm in length and 50mm diameter for the piece 1 and 50 mm in length and 60 mm diameter for the piece 2.

After the necessary processes (machining) required for the fabrication of the pieces by this method the material utilization found for the piece 1 was around 15%, namely near 85% of the material was turned to scrap (metal chips), and for the other piece – near 90% of material turned to scrap. Thus, for the piece 2, only 10% of the material used initially turned into the final product.

The first alternative manufacturing method using the arc welding is performed in two steps. At first, a hollow cylinder is deposited by layers in a direction parallel to its axis. Then the resulting hollow cylinder is rotated by 90˚ and material is deposited around the cylinder to create the flange, Fig. 2.

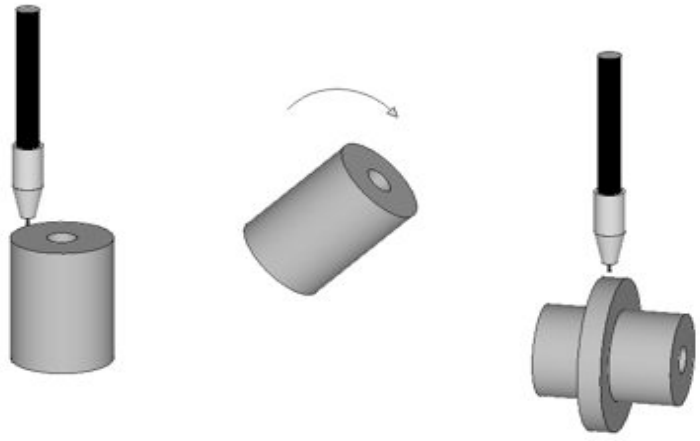

Figure 2. First method of manufacturing by arc welding.

ISSN 2176-5480

Due to the intrinsic error to arc welding processes, the final workpiece has a dimensional allowance up to 2mm. Thus in order to reach the final product a post-processing is required. After a post-processing (e.g. machining), this method proved to be capable of providing the material utilization of approximately 35% for the piece 1 and 34% for the piece 2.

The second method was analyzed considering the flanges already manufactured by traditional processes (sheet-metal stamping or contour milling) with further deposition of material on both sides of the flange, making thus cylindrical part of the body flange (Fig. 3). By this method the use of material was approximately 41% for piece 1 and 44% for piece 2.

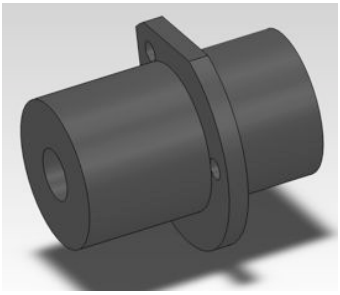

a) Manufacturing of the piece 1

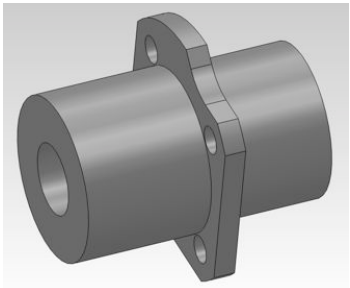

b) Manufacturing of the piece 2

Figure 3. Results of the second manufacturing method by arc welding.

Although the parts are quite small considering the accuracy of the arc welding process (about 50 mm length and 26 mm diameter of body), the two manufacturing methods for welding wasted less material than the traditional process, especially the second method, which uses a combination of metal deposition in successive layers and traditional methods of manufacturing processes, resulting in faster manufacturing and smaller final costs.

3. CASE STUDY

In order to verify the micro and macrostructure of one piece made from the technology studied, as well as mechanical properties of interest, in this item an experimental test of multilayer metal deposition by arc welding is carried out with a stainless steel alloy used in the aerospace engineering area.

3.1 Methodology

A sample prototyping by arc welding is carried out through automated GMAW. The material used for the substrate is the corrosion resistant martensitic stainless steel 9Kh16N4B (also known as EP56) with dimensions 14×104×206 mm. For the multilayer deposition, an austenitic stainless steel (08Kh21N10G6 grade) 1.2 mm diameter wire is used. The chemical compositions of the steels are given in Tab. 1 and Tab. 2.

Table 1. Chemical composition of the substrate stainless steel 9Kh16N4B (alternative name EP56).

Fe	C	Si	Mn	Cr	Ni	Nb	S	P
base	0.08-0.12	< 0.6	< 0.5	15-16.5	4.0-4.5	0.05-0.15	< 0.015	< 0.030

Table 2. Chemical composition of the deposited stainless steel 08Kh21N10G6.

Fe	C	Si	Mn	Cr	Ni	Nb	S	P
base	< 0.10	0.20-0.70	5.0-7.0	20.0-22.0	9.0-11.0	< 0.10	< 0.018	< 0.035

The prototyping is performed in 8 layers in a straight line, when the deposition reaches its maximum length specified (180mm) the welding is interrupted and returns to its starting point to perform the subsequent deposition. The manufactured sample can be seen in Fig. 4 and the geometric data of the dimensions, as well as the welding parameters used can be seen in Tab. 3 and 4.

ISSN 2176-5480

Figure 4. Sample to be studied, manufactured with rapid prototyping by arc welding method (upper sample).

Table 3. Welding parameters.

Current, A	Voltage, V	Wire feed speed, mm/s	Welding speed, mm/min
120	22	58	300

Table 4. Dimensions of the sample.

N° measurement	1	2	3	4	5
Width, mm	10.32	10.86	10.30	9.92	9.72
Height, mm	13.34	14.32	14.32	14.34	16.02
Length, mm	180				
Number of layers	8				

After the layered deposition, the sample must undergo the specific processing necessary for the micro and the macrostructure analyses through an optical microscope.

Thus, the sample was cut by milling in the transverse direction of the weld, using low speed. Abundant cooling was provided to eliminate the possibility of overheating and a possible microstructural change of the piece. After this, the sample was sanded and polished with coarse and fine abrasive fabric, respectively, to obtain a smooth surface. Finally, it was performed an electromechanical polishing with 10% oxalic acid solution and current density near 1A/cm^2.

3.2 Experimental results

The sample macrostructure can be seen in Fig. 5a. Radial strips are initiated in the root bead (first bead) and goes to the upper weld bead. The structure of the beads is not easily distinguished. The fusion lines between beads are diffused and non-contrast. Welding defects such as cracks and spills by the upper weld beads are absent. The heat affected zone (HAZ) is visible under the root bead in the base metal (BM) and has about 2mm thickness. Depth of the weld metal in the base metal (substrate) is approximately 1.5 mm.

ISSN 2176-5480

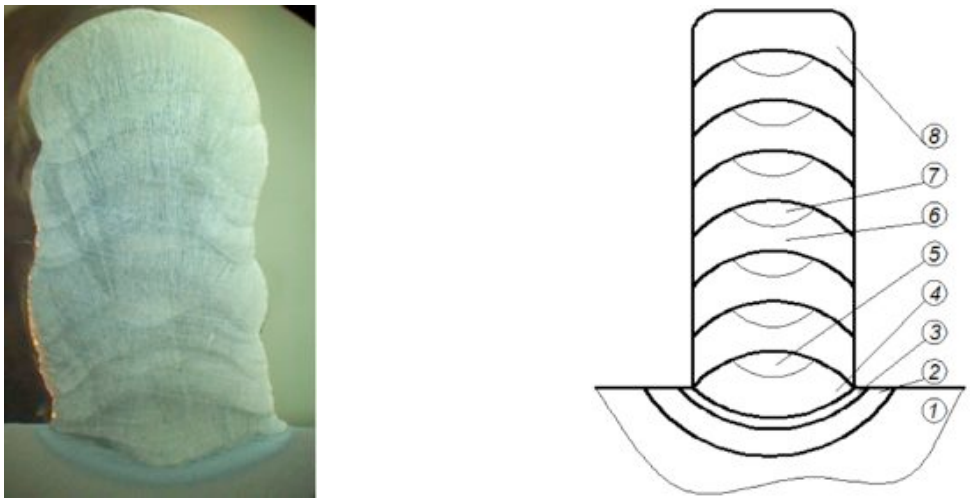

(a) (b)

Figure 5. (a) Picture showing the macrostructure of the sample. (b) Scheme of the sample showing the divisions of the weld beads.

The description of the sample microstructure is given in Tab. 5. A scheme with distinct zones is used to the analysis and description of the sample microstructure, as shown in Fig. 5.

Table 5. Brief description of the sample microstructure

Zone n˚	**Description**	**Microhardness, HRC**
1	Base Metal (substrate): has sorbite structure (superdispersed perlite) with small amount of austenite (Fig. 6). In horizontal direction of the base metal some strips are visible (Fig. 6a).	26
2	Heat affected zone (HAZ), which consists of some regions: 1) The amount of austenite decreases at the lower part of the HAZ, which has greater amount of sorbite, visible at the bottom of Fig. 7a and right of Fig. 7b. 2) Austenite with remnants of non-solved carbides and sorbites prevails close to the center of HAZ (upper left in Fig. 7a and 7b). 3) Austenite (spots) near the weld bead is visible (upper left of Fig. 8a and in the center of Fig. 9a).	39,5
3	Partially melted zone (PMZ): starts with thin strips of austenite and toward the base metal consist of austenite-ferrite phase with presumably eutectic niobium along grain boundary.	--
4	Weld metal: consists of fine austenite-ferrite phase. The structure near the boundary of the base metal looks like columnar dendrite and internally to the weld metal as equiaxed dendrite (Fig. 9d and 10). Strips of an increasing amount of ferrite are visible in some regions near and parallel to the fusion line (Fig. 9c).	26
5	Fusion zone between beads (first and second): has low contrast and has structure of weld metal of the root bead with increased amount of ferrite (dark strips at the Fig. 5a).	--
6	Weld metal of the intermediate beads: have the same structure of the root bead, but with enlarged dendrites (Fig. 11).	< 20
7	Fusion zone between beads of the intermediate steps: have increased amount of austenite (whitening spots at the Fig. 5a). The area of the fusion zone between the beads increases until the center of the sample (having the largest area between the third and fourth bead) and then decreases again until the last bead.	--
8	Weld metal of the last bead: has structure of the root bead with enlarged dendrites.	--

ISSN 2176-5480

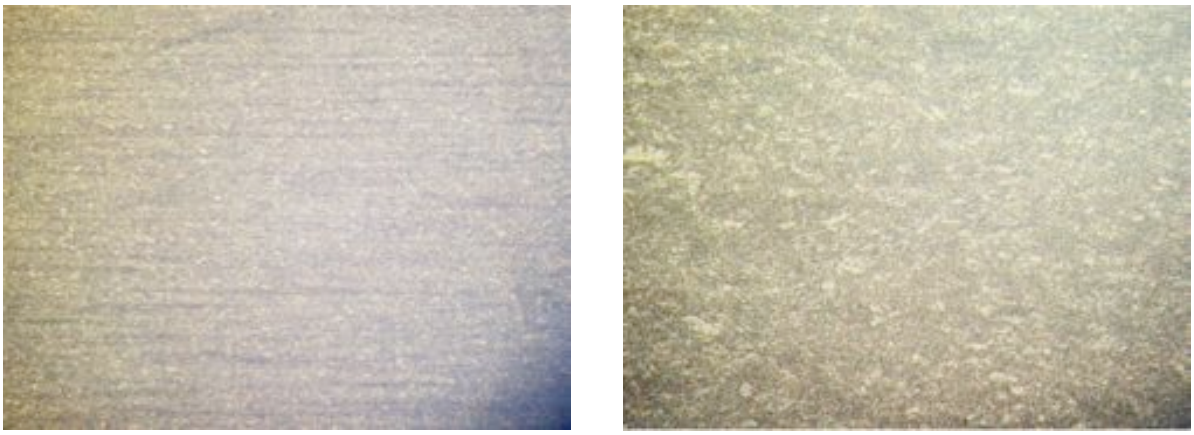

(a) (b)

Figure 6. Microstructure of the base metal, which consists of sorbite (fine pearlite) with a small amount of austenite. a) x63; b) x250.

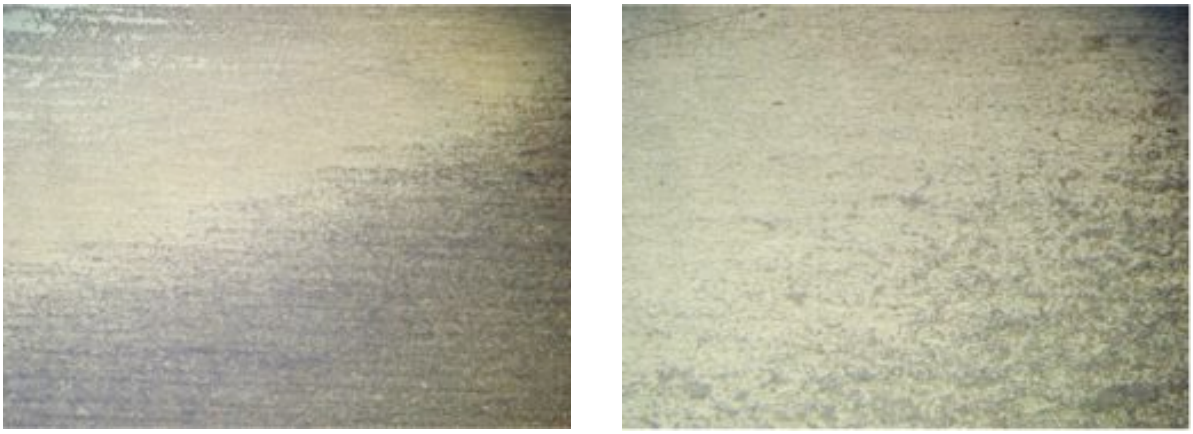

(a) (b)

Figure 7. Microstructure of the metal in the transition zone between the base metal (sorbite with small amounts of austenite) and HAZ (non-solved carbides in austenite and sorbite). a) x63; b) x250.

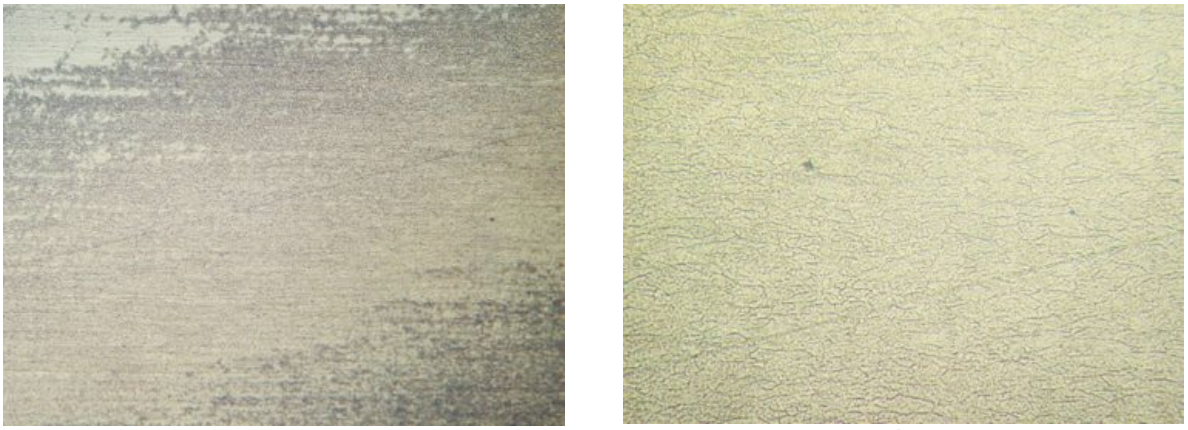

(a) (b)

Figure 8. HAZ microstructure (center – austenite with non-solved carbides and sorbite; upper left – austenite spots). a) x63; b) x250.

ISSN 2176-5480

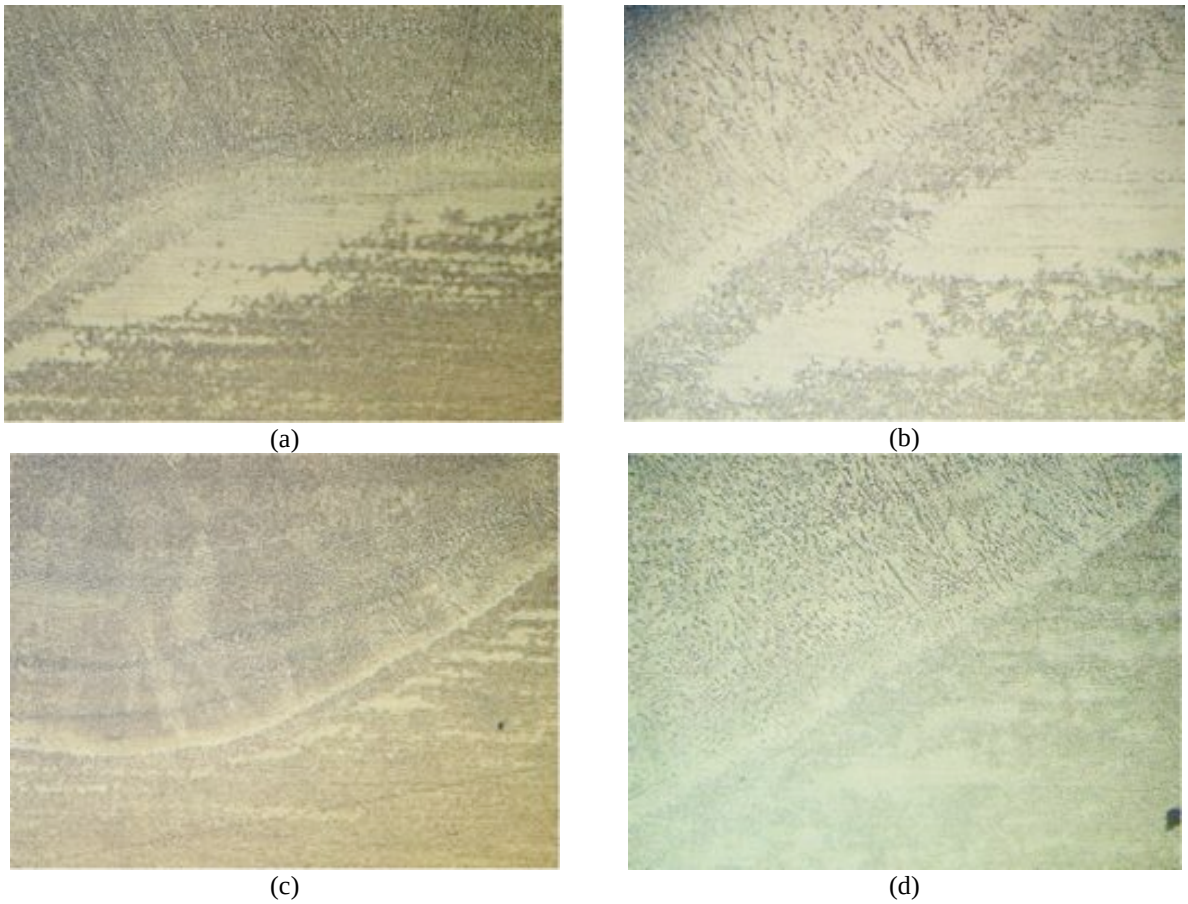

(a) (b)

(c) (d)

Figure 9. Microstructure in the transition zone of the base metal and the root bead (up - columnar dendrite of the weld metal, center - thin austenite strips, down - austenite-sorbite phase with enlarged spots of austenite). a) x63 b) x250.

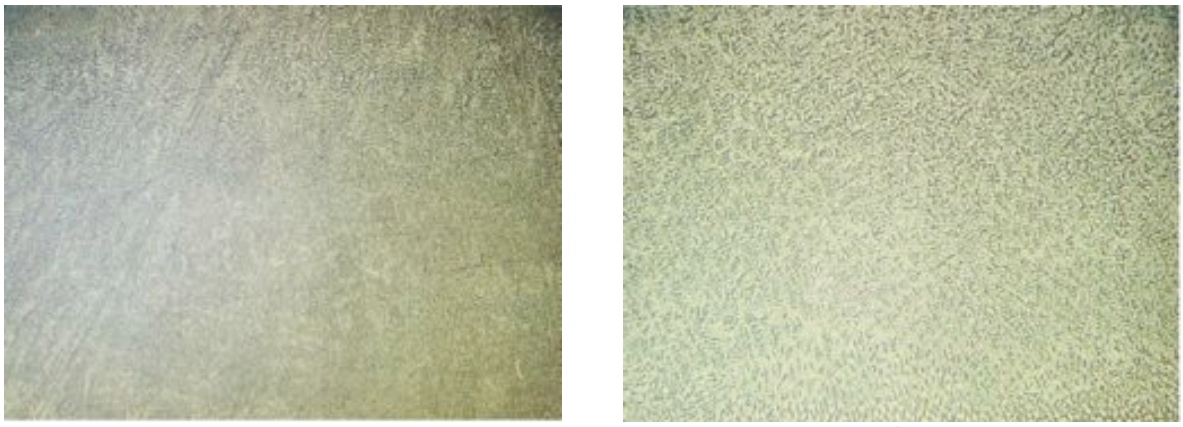

(a) (b)

Figure 10. Microstructure of the root bead (fine austenite-ferrite phase). a) x63; b) x250.

ISSN 2176-5480

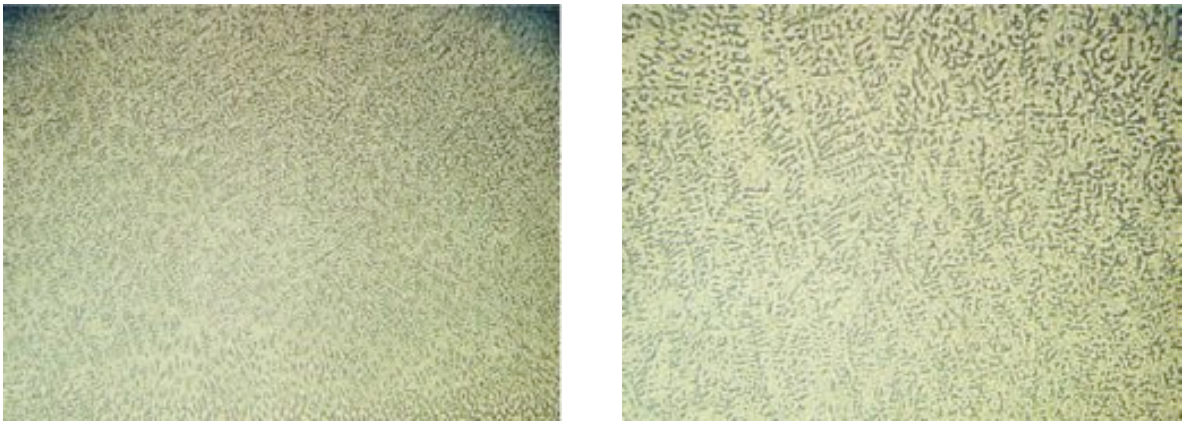

(a) (b)

Figure 11. Microstructure of the 5th bead (austenite-ferrite phase with enlarged dendrites in comparison to the root bead). a) x63; b) x250.

3.3 Interpretation of results

3.3.1 Transcrystalline texture

Presence of radial strips in the weld metal macrostructure is evidence of transcrystalline structure, which is typical for multilayer welding (Медовар, 1954). In transcrystalline structure, columnar grains of each subsequent bead looks like a prolongation of the grains of bottom beads, thus grains grow from one bottom bead to another upper bead. Consequently, the fusion of adjacent beads looks like epitaxial growth (Kou, 2003).

It is important to note that transcrystalline structure remains for both columnar (near fusion line) and equiaxed dendrites. This structure has an important physical content, because it shows the direction of the heat transfer in process of weld deposition.

3.3.2 Base metal

The stripped structure of the base metal (well visible at low magnification) shows the rolling direction of the sheet metal EP56, from which substrate was made.

A sorbite structure (fine perlite) with small amount of austenite is typical for EP56 steel in the annealed state. According to the continuous-cooling transformation (CCT) diagram (taken from EP56 manufacturer certificate), perlite is formed at low cooling rates, which is typical for annealing (Fig. 12). The amount of austenite in the structure is small (less than 10%), which is typical for low-temperature phase state of the studied steel (Tab. 6).

Measured hardness of the base metal is practically the same as for quenching EP56 steel at 950˚C and then tempering at temperature of 600˚C.

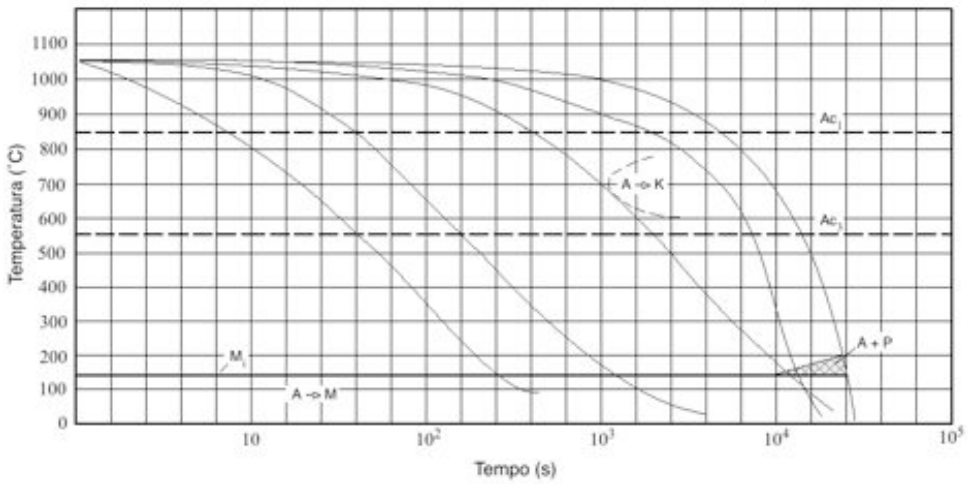

Figure 12. CCT diagram for EP56 steel: Ac_1 – beginning of the austenite transformation; Ac_3 –end of the austenite transformation; A – austenite; k – carbides; Пр. – perlite; Мн – beginning of the martensite transformation; M – martensite (Y – temperature, ˚C; X – time, s)

ISSN 2176-5480

Table 6. Amount of phases in EP56 steel at different temperatures (taken from EP56 manufacturer certificate)

Temperature, °C	Amount of phases, %	
	α-phase	γ-phase
400 - 500	95-97	3-5
550	90	10
600	70	30
650	35	65
700	25	75
750	16	84
800	6	94
850 - 1000	0	100

3.3.3 Heat affected zone

According to the phase diagram (Fig. 12), the heat affected zone (HAZ) consists of several zones (regions) at different temperatures. Considering large cooling rates in the process of weld deposition, it can be said that the phases at normal temperatures are consolidated as phases at temperatures of weld deposition. Thus, the following structures can be observed from base metal to the weld metal: under the point at which the austenization and HAZ begin (550˚C) - sorbite structure with small amounts of austenite; 550 to 850˚C - successive increments at the austenite amount; up to 850˚C - austenite. Austenite-ferrite phase is observed at temperatures close to the melting point, which is typical for Cr-Ni steels with increased amounts of Cr than Ni and, as a result, the primary α-phase is formed at solidification process.

The susceptibility of EP56 steel to fragility is a result of the high hardness of the concerned zone (HRC 39.5) after welding and cooling in environment air (Гольдштейн, 1999). Due to the low amount of carbon in the steel (< 0.1%), this has no relation with increased hardness by carbides forming. Thus, the reason of the possible fragility is connected with the establishing of stressed quenched structures or with the formation of intermetallic compounds such as FeCr (known as σ-phase), which is possible for Cr-Ni steels at temperatures of 650 to 800˚C (Медовар, 1954). These structures, according to EP56 manufacturer data, provide increased hardness at tempering temperatures of 450 to 500˚C.

3.3.4 Partially melted zone

Thin layers of austenite existing in the partially melted zone (PMZ) may be due to diffusion of Ni (also of Mn and Cr) through the ferrite layers. This probably happened because the nickel concentration in weld metal is higher than in the base metal and because the ferrite is less compact than the austenite.

Carbides precipitation at the grain boundaries is a result of increased temperature of NbC dissolution. For example, the dissolution temperature of NbC in Cr-Ni steel 304 is about 1400˚C at carbon amount in steel near 0.1% (Kou, 2003).

The visible δ-phase as a net around the grain boundaries (upper right in Fig. 9b) is the result of high temperature in PMZ, which is typical for primary ferrite solidification. High cooling rate after welding stabilizes this structure.

3.3.5 Weld metal

Austenite-ferrite phase obtained in weld metal is typical for chemical composition of the root bead. Considering the area (in weld bead cross section) of the reinforcement equal to the area of the fusion zone penetration in the base metal, it can be admitted that that the dilution between filler metal and base metal in the weld bead follows a 1:1 ratio. Based on this assumption, the calculated composition of the root bead is shown on Tab. 7.

Table 7. Calculation composition of the root bead with 50% of dissolution.

Metal	Fe	C	Si	Mn	Cr	Ni	Nb	S	P
Base metal	78.7	0.1	0.6	0.5	16	4	0.1	0.015	0.03
Weld metal	62.7	0.1	0.05	6	21	10	0.1	0.018	0.035
Root bead	70.7	0.1	0.33	3.25	18.5	7	0.1	0.017	0.033
Fusion zone between 1˚ and 2˚ bead	66.7	0.1	0.19	4.64	19.75	8.5	0.1	0.017	0.034

According to the Schaeffler diagram (Kou, 2003) for the calculated root bead composition, the austenite-ferrite phase with Cr and Ni equivalents of 19% and 11.6%, respectively, are typical for amounts of ferrite 5-10%.

For such alloys with similar Cr-Ni composition (Fig. 13a) ferrite is the primary phase solidification. Austenite

ISSN 2176-5480

begins to precipitate in the temperature reduction and has a stable phase about 1000-1250˚C. The beginning of carbides and ferrite precipitation from austenite occurs at temperatures lower than 1000˚C. But the real phase diagram of the weld metal is more complicated, that's because influence of Mn was not taken into consideration. Austenite-ferrite phase turns to the austenite region (Fig. 13b) when the amount of Mn increases in Cr-Mn steels.

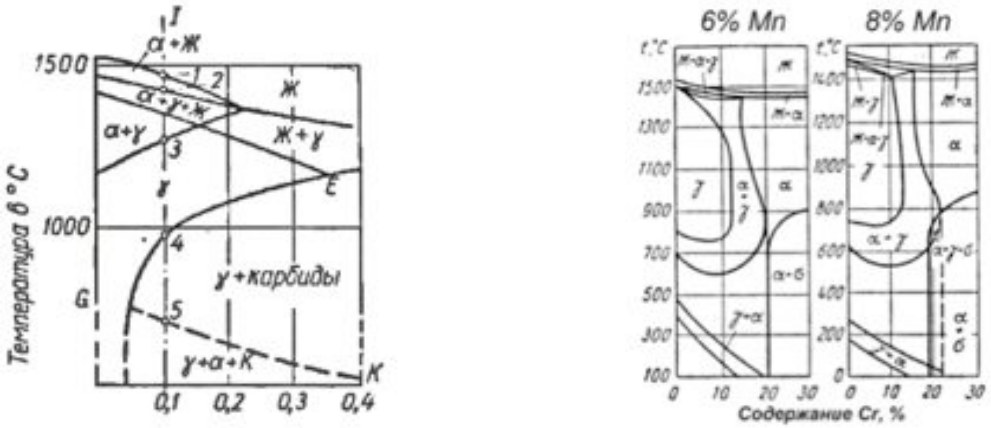

a) b)

Figure 13. Pseudo binary cross-section of a triple phase diagram. a) Fe-Cr-Ni system (Медовар, 1954); b) Fe-Cr-Mn system (Приданцев, 1968) for different amounts of Mn.

Chemical composition from the fourth layer are practically the same of the weld metal, on which Cr and Ni equivalent are close of 21.1% and 16%, respectively. According to the Schaeffler diagram this composition is typical for austenite structure of the weld bead, which can be seen only in the melting zone of adjacent beads (Fig. 14).

In the weld beads of double-phase the visible ferrite is the primary ferrite (Приданцев, 1968). Thus, transformations $\delta \rightarrow \gamma \rightarrow \alpha$, according to Fig. 13a, is not possible on the cooling process of the weld bead. Under this circumstance, the Fe-Cr-Ni-C and Fe-Cr-Ni-Mn-C phase diagrams should be analyzed in more detail, since these diagrams do not take into account high heating and cooling rates.

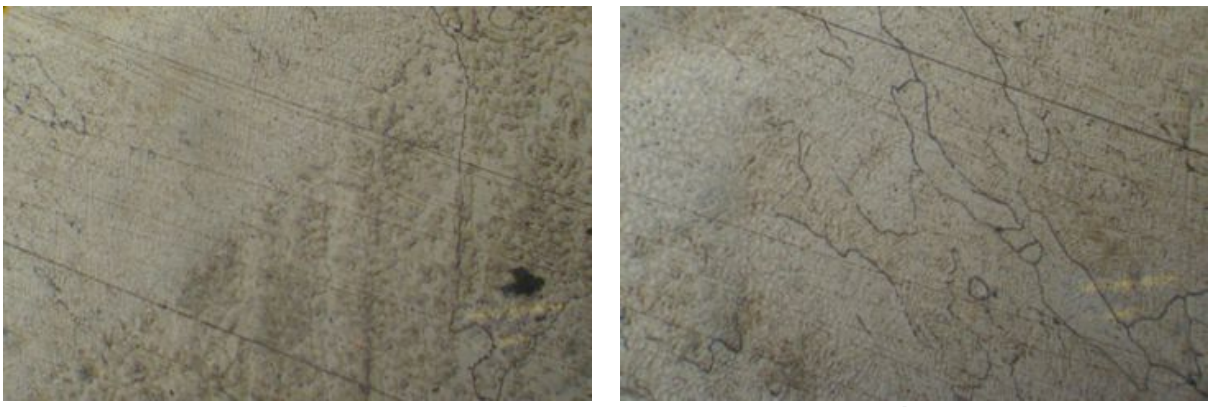

a) b)

Figure 14. Microstructure of the fusion zone between adjacent beads (x300): a) boundary between fusion zone and bead; b) fusion zone.

As a basic rule, in the process of multiple weld deposition there are multiple thermal cycles. In multilayer welding the weld bead number N is not significantly affected by cooling cycles stemmed from beads N+2 due to low temperatures (below 500˚C) (Blondeau, 2008). In the weld bead, several zones can be distinguished (Fig. 15):

- In A zone, the peak temperature is lower than the austenization start point (point Ac_1) - ferrite and carbides are precipitated.
- In B zone the temperature is in the austenization beginning region - increased amount of austenite may be visible.
- In C zone the temperature is in the austenization region (higher temperatures than the complete austenization) - austenite precipitates in regions with large amounts of carbon (as a result of carbides dissolution).

ISSN 2176-5480

- In D zone the temperature is higher than the austenite stability region.

Thus, a region with increased amount of austenite (Fig. 14b) is a result of heating with temperature greater than Ac_3. It is important to note that there are other areas lightly marked in the weld metal, which occurs due to complications of the heat transfer conditions in multilayer welding. Radial growth of dendrites is observed at the top of the micrograph of Fig. 16, which is result of different conditions of heat transfer to different locations of the weld metal.

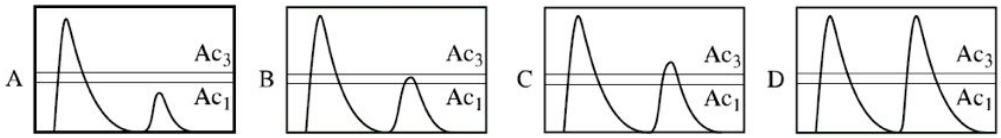

Figure 15. Thermal cycles in weld bead.

Figure 16. Fusion zone of adjacent beads in weld metal.

However, in the middle of the micrograph (Fig. 16) austenite region typical of C zone is observed. Above austenite region is located D zone with increased amount of black spots, a result of δ-phase precipitation at temperatures near the melting point. Below austenite region dark gray spots (A and B zones) are observed as a result of increased precipitation of α-ferrite, carbides and possible σ-phase (σ-phase looks like α-ferrite for the etching method used). Some amount of δ-ferrite appears in that area, but this phase is virtually free of austenite regions. Dendrites of this zone have enlarged dimensions than in the D zone.

Major complications of heat transfer in upper beads are confirmed by the increased size of dendrites (Fig. 10 and 11). This enlargement is more expressed for multilayer samples (Fig. 17).

ISSN 2176-5480

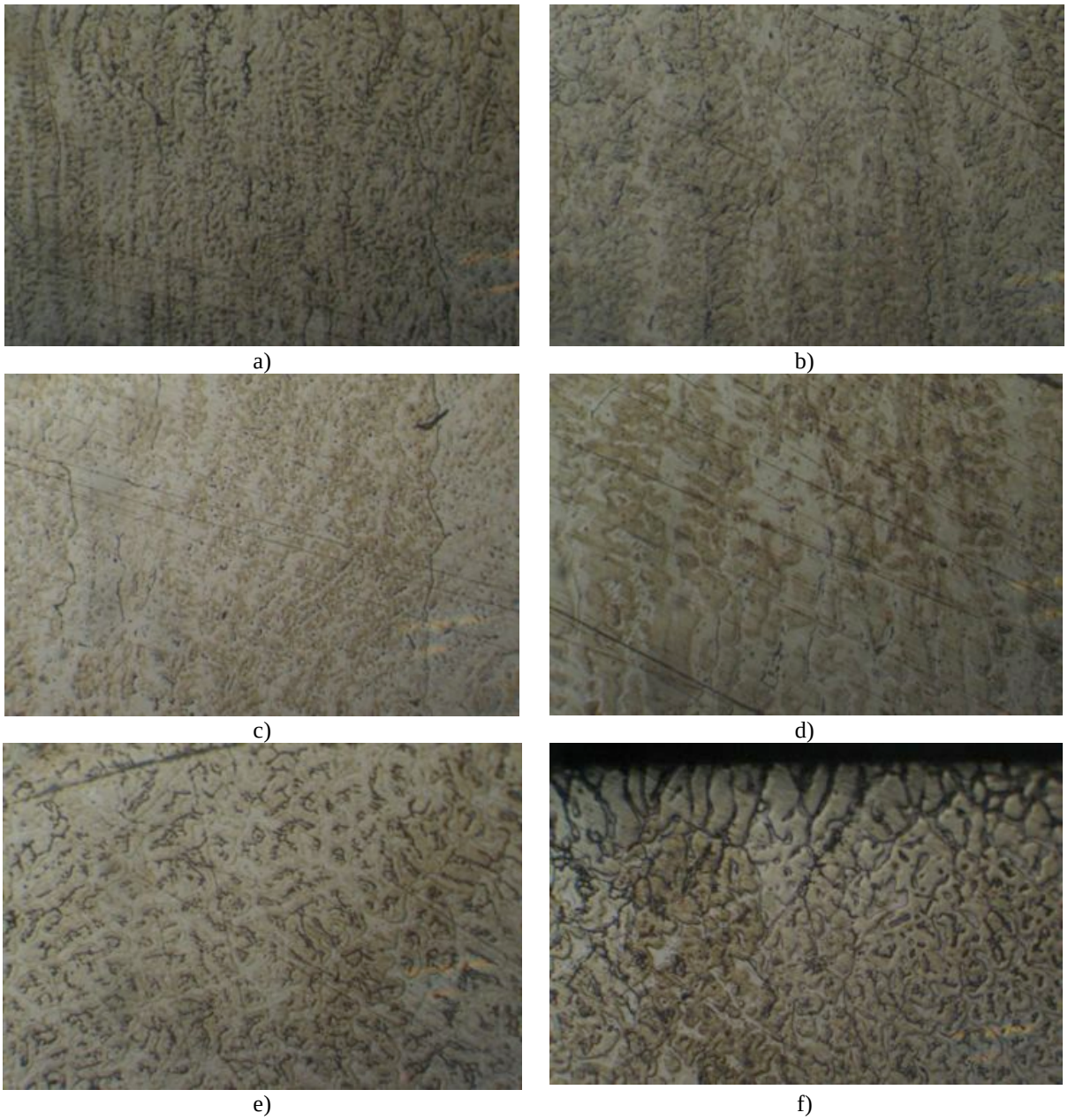

Figure 17. Difference in dendrites dimensions for multilayered sample (x300): a) 1th bead; b) 2th bead; c) 4th bead; d) 6th bead; e) 8th bead; f) outer edge of the 8th bead

4. CONCLUSIONS

The use of rapid prototyping by arc welding with use of high-cost materials, such as for aerospace application, proved advantageous. When compared with traditional methods of manufacturing the use of metal deposition in successive layers wasted much less material than the first. But the use of these two manufacturing methods together showed results even more significant, since in this case the smallest amount of material was wasted.

Although the part to be manufactured were small, the positive result of the use of prototyping by arc welding gives evidence that, for larger dimensions, the waste will be quite small, showing that use of this technology is of great industrial and technological value.

The multiple layer weld deposition, as in the case of rapid prototyping by arc welding seen here, is quite a complicated process that deals with the following effects:

- Multiple heating of the weld beads and the substrate as a result of heat transfer by deposition of the successive beads.
- Complications of weld metal heat transfer with the increasing distance from the substrate surface.
- Different conditions of heating and cooling of the successive beads (as a result there are different preheating

ISSN 2176-5480

conditions).

Thus, the continuous metallographic study of material produced by such processing technology is the most practical way of achieving detailed results, in microscopic levels, so that it can be understood and even predict the mechanical properties found in different parts of a same piece.

5. BIBLIOGRAPHIC REFERENCES

BAUFLED, B. et al. Manufacturing Ti-6Al-4V components by Shaped Metal Deposition: Microstructure and mechanical properties. IOPscience. Trends in Aerospace Manufacturing 2009 International Conference. 2011.

BAUFLED, B.; BIEST, O. V. Mechanical properties of Ti-6Al-4V specimens produced by shaped metal deposition. Katholieke Universiteit Leuven, MTM, Belgium. 2009. Diponível em: <stacks.iop.org/STAM/10/015008>. Acesso em: 11 de junho de 2006.

BLONDEAU, R. Metallurgy and Mechanics of Welding: Process and Industrial Applications. Saint-Etienne: ISTE Ltd., John Wiley & Sons, Inc., p. 496, 2008.

BRANDL, E. et al. Additive Manufactured Ti-6Al-4V Using Welding Wire: Comparison of Laser and Arc Beam Deposition and Evaluation with Respect to Aerospace Material Specifications. ScienceDirect. 2010.

FACHINOTTI, V. D. et al. Evolution of Microstructure During Shaped Metal Deposition. Mecánica Computacional. Buenos Aires, v. 29, p. 4927-4934, nov. 2010.

Kou, S. Welding Metallurgy. 2. ed, Hoboken: John Wiley & Sons, Inc., 2003.

SKIBA, T.; BAUFELD, B.; BIEST, O. V. Microstructure and Mechanical Properties of Stainless Steel Component Manufactured by Shaped Metal Deposition. ISIJ International, v. 49, n. 10, p. 1588-1591, 2009.

THUKARAM, S. K. Robot Based 3D Welding for Jet Engine Blade Repair and Rapid Prototyping of Small Components. 120 p. Thesis for the degree of master of science. Department of Mechanical and manufacturing Engineering, University of Manitova Winnipeg, Manitova, Canada. 2010.

VOLPATO, N. et al. Prototipagem Rápida – Tecnologias e Aplicações. 1. ed. São Paulo: Edgar Blücher, v. 1, p. 244, 2007.

ZHANG, Y. M. et al. Automated system for welding-based rapid prototyping. Department of Electrical Engineering and Center for Robotics and Manufacturing Systems, College of Engineering, University of Kentucky, Lexington, KY 40508, USA. 2002.

Гольдштейн, М.И.; Грачев, С.В.; Векслер, Ю.Г. Специальные стали: Учебник для вузов, 2-еизд. М: МИСИС, 408 с, 1999.

Медовар, Б.И. Сварка Хромоникелевых аустенитных сталей. К.: Машгиз, 175 с, 1954 г.

Приданцев, М.В.; Талов, Н.П.; Левин, Ф.Л. Высокопрочные аустенитные стали. М.: Металлургия, 1968. – 248 с.

6. RESPONSIBILITY NOTICE

The authors are the only responsible for the printed material included in this paper.